Higgs Boson production in association with jets in gluon-gluon fusion

G Luisoni[1], N Greiner[2], S Höche[3], M Schönherr[2], J Winter[4] and V Yundin[5]

[1] Theoretical Physics Department, CERN, Geneva, Switzerland
[2] Physik-Institut, Universität Zürich, Winthertherstrasse 190, CH-8057 Zürich, Switzerland
[3] SLAC National Accelerator Laboratory, Menlo Park, CA 94025, USA
[4] Department of Physics and Astronomy, Michigan State University, East Lansing, MI 48824, USA
[5] Max-Planck-Institut für Physik, Föhringer Ring 6, D-80805 München, Germany

E-mail: gionata.luisoni@cern.ch

Abstract. We present the computation of the NLO QCD corrections to the production of a Standard Model Higgs boson in association with up to three jets through gluon-gluon fusion. The computation is performed in the approximation of an infinitely heavy top quark. Before studying some phenomenologically important observables, we describe some technical detail about the computation.

1. Introduction

A major step after the discovery of the Higgs particle [1, 2] is the precise determination of its nature. Among the important properties, besides spin and parity, there are its couplings to fermions and other bosons. In order to discriminate between the electroweak symmetry breaking mechanism in the Standard Model and possible Beyond Standard Model scenarios, measurements have to be compared with very precise predictions.

The main Higgs boson production mechanism is given by the gluon fusion channel, where the Higgs boson is produced out of two initial state gluons via a loop of heavy quarks. The presence of two gluon in the initial state enhances the tendency of producing further QCD radiation in this production channel, where also higher order corrections are very large. For this reason they were recently computed to N^3LO [3]. The unavoidable presence of further jets makes the gluon fusion mechanism an interesting process on its own, in particular to study the Higgs boson in a very jetty environment. However, it is also an irreducible background to another very important production channel, namely vector boson fusion (VBF).

During Run II at the LHC, the VBF mechanism will play a leading role. In this production mode, a Higgs boson is created by annihilation of virtual W or Z bosons, radiated off the initial-state (anti-)quarks in a t-channel scattering process with no color exchange at leading order [4, 5]. This allows to directly probe the couplings between the Higgs boson and the electroweak gauge bosons providing at the same time a clean signature consisting of two forward jets and only little hadronic energy between these tagging jets.

In order to discriminate between these two production mechanisms it is crucial to be able to estimate the contamination of gluon fusion events in the VBF sample, and to devise the best

selection strategies, which allow to keep untertainties under control providing at the same time the highest signal-to-background ratios.

In this talk we discuss the calculation and the phenomenlogy of the production of a Standard Model Higgs boson in association up to three jets, as described in detail in the references [6–8]. The calculation takes into account next-to-leading order QCD corrections and is carried out in the limit of an infinitely heavy top quark. We discuss two different sets of cuts: a set of basic cuts that are suitable for the gluon fusion contribution and a more restrictive set of cuts, which mimics the one adopted in VBF analyses. In addition we discuss different schemes for defining the tagging jets.

2. Computational setup

2.1. The codes

The computation is performed using the automated tools GoSam [9, 10] and Sherpa [11], linked via the interface defined in the Binoth Les Houches Accord [12, 13].

The one-loop amplitudes are generated with the new version 2.0 of GoSam, and are based on an algebraic generation of d-dimensional integrands using a Feynman diagrammatic approach. The expressions for the amplitudes are generated employing QGraf [14], Form [15, 16] and Spinney [17]. For the reduction of the tensor integrals at running time we used Ninja [18, 19], which is an automated package carrying out the integrand reduction via Laurent expansion [20], and OneLoop [21] for the evaluation of the scalar integrals. Unstable phase space points are detected automatically and reevaluated with the tensor integral library Golem95 [22–24]. Alternatively, one can use other reduction techniques such as the standard OPP method [25–27] as implemented in Samurai [28]. All the reduction programs had to be upgraded in order to be able to deal with the higher rank loop integrals generated by the presence of the effective gluon-gluon-Higgs boson vertex.

The calculation of tree-level matrix elements for the Born and the real emission contribution as well as the subtraction terms in the Catani-Seymour approach [29] have been done within Sherpa using the matrix element generator Comix [30]. These amplitudes were validated using a combination of MadGraph 4 [31, 32], MadDipole [33, 34] and MadEvent [35]

2.2. Root *Ntuples*

Because of the relatively slow NLO computation and the high statistics needed for such a large multiplicity final state, the Monte Carlo events are stored in the form of Root Ntuples. They are generated by Sherpa and were first used in the context of vector boson production in association with jets [36].

For this calculation, sets of Ntuples files with Born (B), virtual (V), integrate subtraction terms (I) and real minus subtraction term (RS) type of events have been generated for H + 1 jet, H + 2 jets and H + 3 jets at the center-of-mass energies of 8, 13, 14 and 100 TeV. The events were generated such that jets can be clustered using the k_T or anti-k_T algorithm [37, 38] as implemented in the FastJet package [39] and with radii that can vary between $R = 0.1$ and $R = 1$. On the jets a minimal generation cut was imposed by requiring $p_T > 25$ GeV, $|\eta| < 4.5$, which allow to post-process the events in every analysis with more inclusive cuts.

2.3. Analysis cuts and parameter settings

We present here results for two center of mass energies at 8 and 13 TeV. In both cases we have applied two sets of cuts: a baseline set with minimal cuts to render the cross section finite, and a more restrictive set of cuts, which is typically used in the context of VBF searches. In both cases jets are clustered using the anti-k_T algorithm [37, 38] as implemented in the FastJet package [39]. If not specified explicitly, the jet radius and PDF set have been set to $R = 0.4$ and CT10nlo [41], respectively. The baseline set consists of the following cuts: $p_T > 30$ GeV,

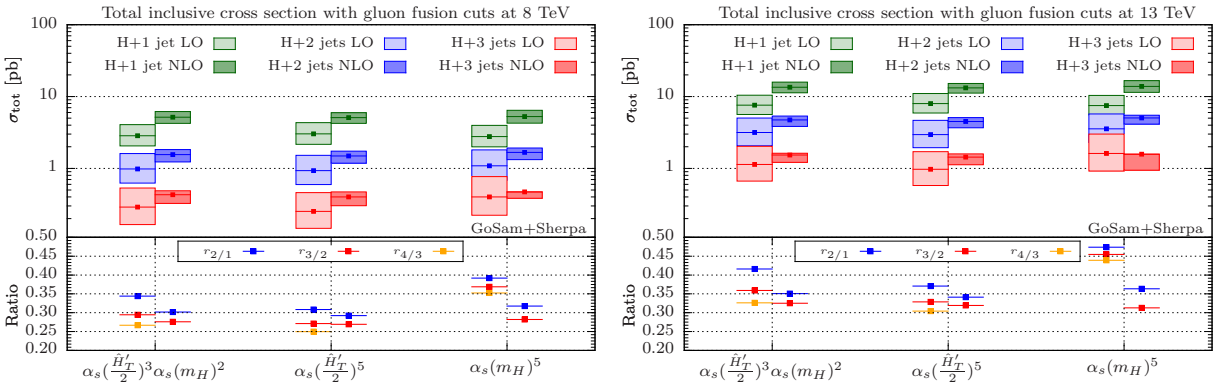

Figure 1: Total cross sections at LO (left side of each column) and NLO (right side of each column) for $\mathrm{H}+1\,\mathrm{jet}$ (green), $\mathrm{H}+2\,\mathrm{jets}$ (blue) and $\mathrm{H}+3\,\mathrm{jets}$ (red) production using the three different scale choices as explained in text. In the lower part of the plots, the ratios $r_{2/1}$ (blue), $r_{3/2}$ (red) and $r_{4/3}$ (orange) are shown. Results have been obtained for 8 TeV and 13 TeV (left and right plot respectively).

$|\eta| < 4.4$. In the VBF case two additional cuts have been imposed, given by $m_{j_1 j_2} > 400$ GeV, $|\Delta y_{j_1,j_2}| > 2.8$. Here the two jets, j_1 and j_2, denote the tagging jets. Their selection is not unique and we study two different schemes, one where the two tagging jets are the two jets with the highest p_T (p_T-tagging), and one where the most forward and most backward jet (in rapidity) yield the two tagging jets (y-tagging).
The central scale for the renormalization and the factorization scale is chosen to be

$$\mu_F = \mu_R \equiv \frac{\hat{H}'_T}{2} = \frac{1}{2}\left(\sqrt{m_H^2 + p_{T,H}^2} + \sum_i |p_{T,i}|\right) . \tag{1}$$

However it is not obvious whether this dynamical scale is also a good choice to be used for the gluon-gluon-Higgs coupling. One might argue that the Higgs mass is the appropriate scale there. Therefore we consider three different scale choices, defined as

$$\mathrm{A}: \quad \alpha_\mathrm{s}\left(x \cdot \frac{\hat{H}'_T}{2}\right)^3 \alpha_\mathrm{s}\left(x \cdot m_H\right)^2 , \qquad \mathrm{B}: \quad \alpha_\mathrm{s}\left(x \cdot \frac{\hat{H}'_T}{2}\right)^5 , \qquad \mathrm{C}: \quad \alpha_\mathrm{s}\left(x \cdot m_H\right)^5 . \tag{2}$$

The presence of the factor x indicates that this scale is varied in the range $x \in [0.5, \ldots, 2]$.

3. Numerical results for gluon fusion setup

We start the discussion of the numerical results with the basic gluon fusion cuts. One of the most important observables is the total cross section. In figure 1 we report the total cross sections for both leading order and next-to-leading order for the processes $\mathrm{H}+1\,\mathrm{jet}$, $\mathrm{H}+2\,\mathrm{jets}$ and $\mathrm{H}+3\,\mathrm{jets}$ at $E_\mathrm{cm} = 8$ TeV (left plot) and $E_\mathrm{cm} = 13$ TeV (right plot). The results are shown for the three scale choices described above. On the level of total cross sections one only observes a mild dependence on the scale choice, in particular for the NLO results. For the fixed scale one observes an enhancement of the LO ratios. An increase of the center of mass energy from 8 to 13 TeV also only has a small influence on the overall pattern. The situation is different when one looks at differential distributions. In figure 2 we show the transverse momentum distribution for the Higgs boson for the $\mathrm{H}+3\,\mathrm{jets}$ process at a center of mass energy of 8 TeV.

The subplot on the right shows the distribution for scale choice B, while Fig. 2a shows the results for the different scales normalized to the NLO result of scale A. The advantage of scale B is the flatness of the K-factor over the entire p_T range. This supports our choice to make scale

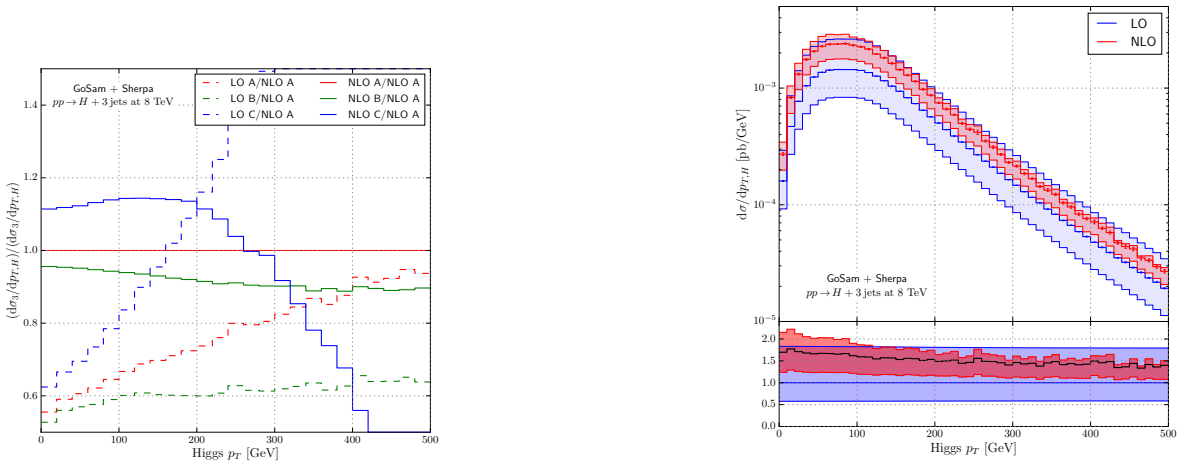

(a) Ratio

(b) Scale choice B

Figure 2: On the right: the p_T distribution of the Higgs boson in H + 3 jets production at the 8 TeV LHC presented for scale B. The subplot 2a shows the same central predictions normalized to the NLO result for scale A. Each ratio plot depicts the respective differential K-factors and their envelopes obtained from scale variations at LO and NLO.

B the default scale. For the lower p_T region up to $\sim$ 250 GeV, scale C seems to be a sensible choice as well. However, it completely breaks down for higher p_T, and the K-factor can even become negative. Further support for using scale B as the default choice comes from looking at the p_T distribution of the 'wimpiest' jet for each multiplicity. This means looking at the first jet for H + 1 jet, at the second jet for H + 2 jets, and at the third jet for H + 3 jets. This is illustrated in figure 3. The left hand side shows the p_T of the three jets for scale choice B, the right hand side shows scale choice A. The lower part of the plots shows the ratio of NLO versus LO for each jet. For better visibility the ratios are multiplied with a prefactor to avoid overlap of the bands of the different jets. As can be seen from the ratio plots, the purely dynamical scale choice B leads to flat K-factors, whereas scale choice A shows a decrease of the K-factor with increasing transverse momentum.

Another interesting question is how observables that are defined independently of a certain jet multiplicity, like the transverse momentum of the Higgs, change under the presence of additional QCD radiation. This is shown in figure 4. The upper plots show the NLO distributions for one, two and three jets (which we have obtained from the one-jet, two-jet and three-jet NLO calculations, respectively). Unless stated otherwise, the jet multiplicity is exclusive, labelled by 'excl', i.e. a veto on any additional jet activity is in place. The 1-jet and the 3-jet processes are shown twice, once for the exclusive case, and once for the inclusive case, labelled by 'incl'. The lower subpanels show each contribution normalized to the inclusive prediction of the core process, i.e. the most inclusive one, here given by the H + 1 jet process. The plots in the middle and lower panel are constructed following the same principle but using the NLO core process of increased jet multiplicity, namely H + 2 jets and H + 3 jets, respectively. The middle row of figure 4 hence depicts the same situation but without accounting for the H + 1 jet process; and, for the lower row, there are only two distributions left to show, the one for the exclusive and the one for the inclusive H + 3 jets process. One can see that the low energy region is dominated by the exclusive H + 1 jet contribution. The H + 2 jets contribution is negligible in that region, however starts to dominate already in a region above approx. 200 GeV. Going further up in

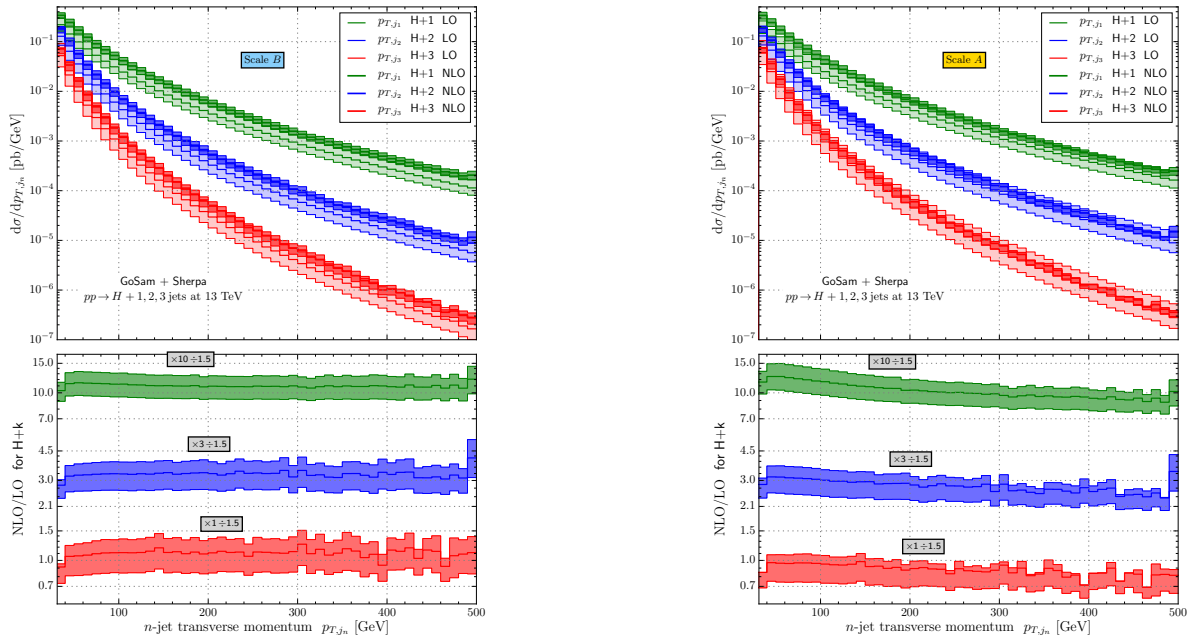

Figure 3: Transverse momentum distribution of the 'wimpiest' jet in $\mathrm{H}+n$ jets production at the LHC. Using p_T ordering the first, second and third leading jet are shown in $\mathrm{H}+1$ jet, $\mathrm{H}+2$ jets and $\mathrm{H}+3$ jets at 13 TeV, respectively; on the left with the default scale choice B, on the right with the scale choice A.

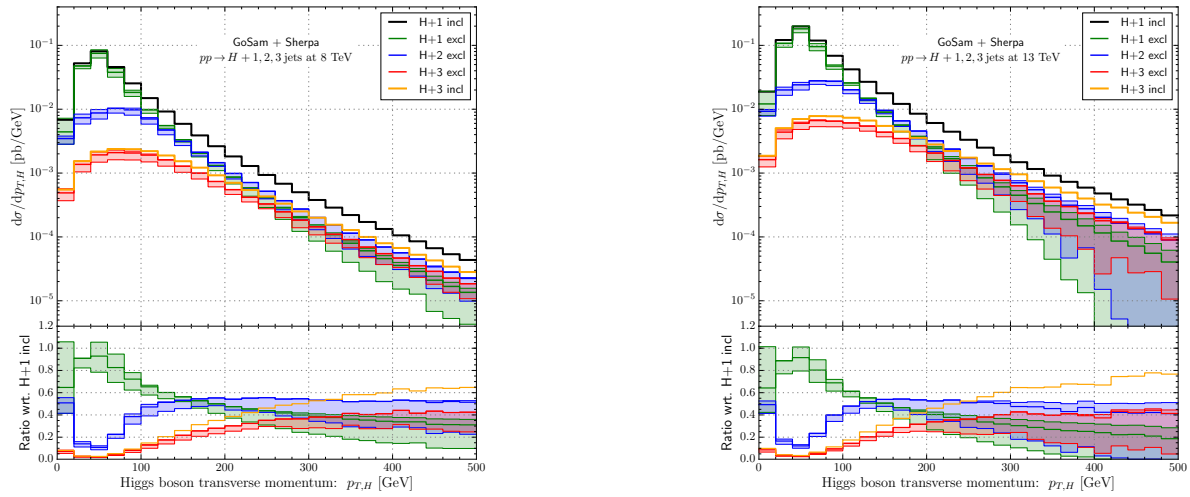

Figure 4: Transverse momentum distribution of the Higgs for the different jet multiplicities. L.h.s. shows the result for 8 TeV, r.h.s. shows the distribution for 13 TeV.

the spectrum increases the $\mathrm{H}+3$ jets contribution which will eventually dominate the spectrum. In other words, at high enough energies it is more and more likely to produce further jets. This has to be kept in mind when comparing an inclusive measurement with a fixed order calculation for a given number of jets. For low multiplicities the description becomes inaccurate already at relatively low energies of around 200 GeV. A theoretical prediction that is based on a merged result of different multiplicities will yield a better description of the data.

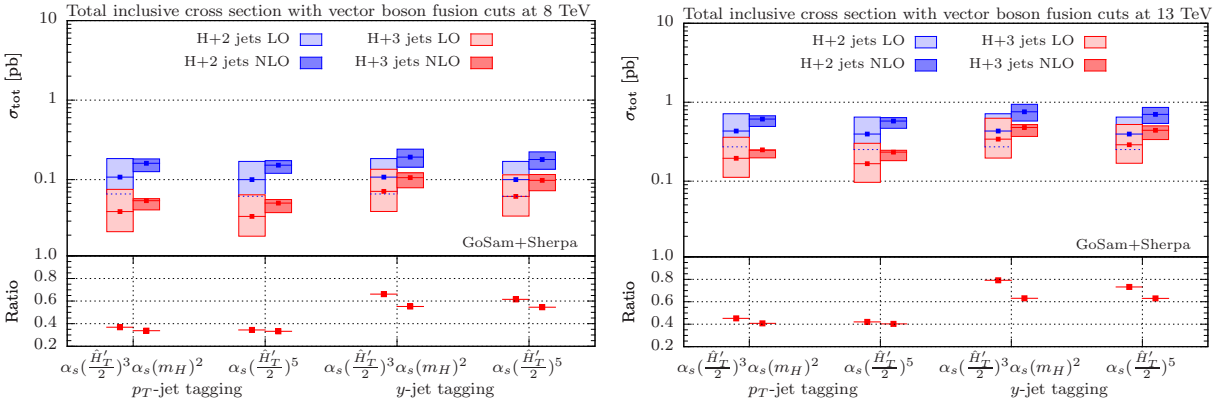

Figure 5: Total cross sections at LO and NLO for H + 2 jets (blue) and H + 3 jets (red) using VBF kinematical cuts and two different tagging jet definitions. Results are shown for the two scale choices A and B, as well as the two energies of 8 TeV (left plot) and 13 TeV (right plot). The lower part of each plot depicts the inclusive cross section ratios $r_{3/2}$ for the different scales and tag jet approaches.

4. Phenomenology with vector boson fusion cuts

As already mentioned, gluon fusion is an irreducible background to the VBF channel. A challenging task is therefore to provide a precise prediction of its rate compared to the signal. In this section we discuss the results obtained from the gluon fusion contribution under the presence of the additional VBF cuts described in section 2.3. Again we start the discussion with the total cross section, for the VBF selection we now also consider the differences between the two tagging schemes described above, p_T-tagging and y-tagging. The total cross section for the different energies, scales and tagging schemes is shown in figure 5. Having ruled out the fixed scale as a sensible choice we only show the result for the two scales A and B. Also in the case of the VBF selection, the differences between the scale choices are rather small. The tagging scheme has a much bigger impact. The y-tagging increases the ratios which means that it increases the fraction of the processes with higher multiplicity. This stresses the importance of the inclusion of NLO results with higher multiplicities into the theoretical prediction.

5. Conclusions

In this talk we presented the computation and some phenomenological results for the production of a Standard Model Higgs boson via the gluon fusion mechanism in the heavy top mass limit in association with up to three jets. We investigated the role of the scale choice as well as the effects of different sets of cuts, also allowing to assess the role of the gluon fusion contribution in VBF searches. Furthermore we discussed a variety of important observables allowing for a better discrimination between the gluon fusion and vector boson fusion contribution. Further improvements could certainly be achieved by providing a merged NLO result of the different jet multiplicities, but also through the inclusion of top-quark mass effects as well as the matching of the H + 3 jets NLO result with a parton shower.

Acknowledgments

We would like to thank the members of the GoSam collaboration for their help and effort. NG was supported by the Swiss National Science Foundation under contract PZ00P2_154829. This research used computing resources from the Rechenzentrum Garching.

References

[1] Aad G *et al.* (ATLAS Collaboration) 2012 *Phys.Lett.* **B716** 1–29 (*Preprint* 1207.7214)

[2] Chatrchyan S *et al.* (CMS Collaboration) 2012 *Phys.Lett.* **B716** 30–61 (*Preprint* 1207.7235)
[3] Anastasiou C, Duhr C, Dulat F, Furlan E, Gehrmann T, Herzog F, Lazopoulos A and Mistlberger B 2016 (*Preprint* 1602.00695)
[4] Cahn R and Dawson S 1984 *Phys.Lett.* **B136** 196
[5] Kane G L, Repko W and Rolnick W 1984 *Phys.Lett.* **B148** 367–372
[6] Greiner N, Hoeche S, Luisoni G, Schoenherr M, Winter J C and Yundin V 2016 *JHEP* **01** 169 (*Preprint* 1506.01016)
[7] Cullen G, van Deurzen H, Greiner N, Luisoni G, Mastrolia P *et al.* 2013 *Phys.Rev.Lett.* **111** 131801 (*Preprint* 1307.4737)
[8] van Deurzen H, Greiner N, Luisoni G, Mastrolia P, Mirabella E *et al.* 2013 *Phys.Lett.* **B721** 74–81 (*Preprint* 1301.0493)
[9] Cullen G, Greiner N, Heinrich G, Luisoni G, Mastrolia P *et al.* 2012 *Eur.Phys.J.* **C72** 1889 (*Preprint* 1111.2034)
[10] Cullen G, van Deurzen H, Greiner N, Heinrich G, Luisoni G *et al.* 2014 *Eur.Phys.J.* **C74** 3001 (*Preprint* 1404.7096)
[11] Gleisberg T, Höche S, Krauss F, Schönherr M, Schumann S *et al.* 2009 *JHEP* **0902** 007 (*Preprint* 0811.4622)
[12] Binoth T, Boudjema F, Dissertori G, Lazopoulos A, Denner A *et al.* 2010 *Comput.Phys.Commun.* **181** 1612–1622 (*Preprint* 1001.1307)
[13] Alioli S, Badger S, Bellm J, Biedermann B, Boudjema F *et al.* 2014 *Comput.Phys.Commun.* **185** 560–571 (*Preprint* 1308.3462)
[14] Nogueira P 1993 *J.Comput.Phys.* **105** 279–289
[15] Vermaseren J A M 2000 (*Preprint* math-ph/0010025)
[16] Kuipers J, Ueda T, Vermaseren J and Vollinga J 2013 *Comput.Phys.Commun.* **184** 1453–1467 (*Preprint* 1203.6543)
[17] Cullen G, Koch-Janusz M and Reiter T 2011 *Comput.Phys.Commun.* **182** 2368–2387 (*Preprint* 1008.0803)
[18] van Deurzen H, Luisoni G, Mastrolia P, Mirabella E, Ossola G *et al.* 2014 *JHEP* **1403** 115 (*Preprint* 1312.6678)
[19] Peraro T 2014 *Comput.Phys.Commun.* **185** 2771–2797 (*Preprint* 1403.1229)
[20] Mastrolia P, Mirabella E and Peraro T 2012 *JHEP* **1206** 095 (*Preprint* 1203.0291)
[21] van Hameren A 2011 *Comput.Phys.Commun.* **182** 2427–2438 (*Preprint* 1007.4716)
[22] Heinrich G, Ossola G, Reiter T and Tramontano F 2010 *JHEP* **1010** 105 (*Preprint* 1008.2441)
[23] Binoth T, Guillet J P, Heinrich G, Pilon E and Reiter T 2009 *Comput.Phys.Commun.* **180** 2317–2330 (*Preprint* 0810.0992)
[24] Cullen G, Guillet J P, Heinrich G, Kleinschmidt T, Pilon E *et al.* 2011 *Comput.Phys.Commun.* **182** 2276–2284 (*Preprint* 1101.5595)
[25] Ossola G, Papadopoulos C G and Pittau R 2007 *Nucl. Phys.* **B763** 147–169 (*Preprint* hep-ph/0609007)
[26] Mastrolia P, Ossola G, Papadopoulos C and Pittau R 2008 *JHEP* **0806** 030 (*Preprint* 0803.3964)
[27] Ossola G, Papadopoulos C G and Pittau R 2008 *JHEP* **0805** 004 (*Preprint* 0802.1876)
[28] Mastrolia P, Ossola G, Reiter T and Tramontano F 2010 *JHEP* **1008** 080 (*Preprint* 1006.0710)
[29] Catani S and Seymour M H 1997 *Nucl. Phys.* **B485** 291–419 (*Preprint* hep-ph/9605323)
[30] Gleisberg T and Höche S 2008 *JHEP* **0812** 039 (*Preprint* 0808.3674)
[31] Stelzer T and Long W F 1994 *Comput. Phys. Commun.* **81** 357–371 (*Preprint* hep-ph/9401258)
[32] Alwall J *et al.* 2007 *JHEP* **09** 028 (*Preprint* 0706.2334)
[33] Frederix R, Gehrmann T and Greiner N 2008 *JHEP* **09** 122 (*Preprint* 0808.2128)
[34] Frederix R, Gehrmann T and Greiner N 2010 *JHEP* **1006** 086 (*Preprint* 1004.2905)
[35] Maltoni F and Stelzer T 2003 *JHEP* **02** 027 (*Preprint* hep-ph/0208156)
[36] Bern Z, Dixon L J, Febres Cordero F, Hoeche S, Ita H, Kosower D A and Maitre D 2014 *Comput. Phys. Commun.* **185** 1443–1460 (*Preprint* 1310.7439)
[37] Cacciari M and Salam G P 2006 *Phys.Lett.* **B641** 57–61 (*Preprint* hep-ph/0512210)
[38] Cacciari M, Salam G P and Soyez G 2008 *JHEP* **04** 063 (*Preprint* 0802.1189)
[39] Cacciari M, Salam G P and Soyez G 2012 *Eur.Phys.J.* **C72** 1896 (*Preprint* 1111.6097)
[40] Hamilton K, Nason P and Zanderighi G 2012 *JHEP* **1210** 155 (*Preprint* 1206.3572)
[41] Lai H L, Guzzi M, Huston J, Li Z, Nadolsky P M *et al.* 2010 *Phys.Rev.* **D82** 074024 (*Preprint* 1007.2241)